Anticancer Chemosensitization and Radiosensitization by the Novel Poly(ADP-ribose) Polymerase-1 Inhibitor AG14361

Christopher R. Calabrese, Robert Almassy, Stephanie Barton, Michael A. Batey, A. Hilary Calvert, Stacie Canan-Koch, Barbara W. Durkacz, Zdenek Hostomsky, Robert A. Kumpf, Suzanne Kyle, Jianke Li, Karen Maegley, David R. Newell, Elena Notarianni, Ian J. Stratford, Donald Skalitzky, Huw D. Thomas, Lan-Zhen Wang, Stephen E. Webber, Kaye J. Williams, Nicola J. Curtin

Background: **Poly(ADP-ribose) polymerase-1 (PARP-1) facilitates the repair of DNA strand breaks. Inhibiting PARP-1 increases the cytotoxicity of DNA-damaging chemotherapy and radiation therapy *in vitro.* Because classical PARP-1 inhibitors have limited clinical utility, we investigated whether AG14361, a novel potent PARP-1 inhibitor (inhibition constant <5 n*M*), enhances the effects of chemotherapy and radiation therapy in human cancer cell cultures and xenografts.** ***Methods:*** **The effect of AG14361 on the antitumor activity of the DNA alkylating agent temozolomide, topoisomerase I poisons topotecan or irinotecan, or x-irradiation or γ-radiation was investigated in human cancer cell lines A549, LoVo, and SW620 by proliferation and survival assays and in xenografts in mice by tumor volume determination. The specificity of AG14361 for PARP-1 was investigated by microarray analysis and by antiproliferation and acute toxicity assays in PARP-$1^{-/-}$ and PARP-$1^{+/+}$ cells and mice. After intraperitoneal administration, the concentration of AG14361 was determined in mouse plasma and tissues, and its effect on PARP-1 activity was determined in tumor homogenates. All statistical tests were two-sided.** ***Results:*** **AG14361 at 0.4 μ*M* did not affect cancer cell gene expression or growth, but it did increase the antiproliferative activity of temozolomide (e.g., in LoVo cells by 5.5-fold, 95% confidence interval [CI] = 4.9-fold to 5.9-fold; *P* = .004) and topotecan (e.g., in LoVo cells by 1.6-fold, 95% CI = 1.3-fold to 1.9-fold; *P* = .002) and inhibited recovery from potentially lethal γ-radiation damage in LoVo cells by 73% (95% CI = 48% to 98%).** ***In vivo,*** **nontoxic doses of AG14361 increased the delay of LoVo xenograft growth induced by irinotecan, x-irradiation, or temozolomide by two- to threefold. The combination of AG14361 and temozolomide caused complete regression of SW620 xenograft tumors. AG14361 was retained in xenografts in which PARP-1 activity was inhibited by more than 75% for at least 4 hours.** ***Conclusion:*** **AG14361 is, to our knowledge, the first high-potency PARP-1 inhibitor with the specificity and *in vivo* activity to enhance chemotherapy and radiation therapy of human cancer. [J Natl Cancer Inst 2004;96:56–67]**

Poly(ADP-ribose) polymerase-1 (PARP-1, EC 2.4.2.30) is an abundant 116-kd nuclear enzyme that is constitutively expressed. It is the first and most extensively characterized member of an expanding family of PARP enzymes *(1)*. In response to DNA strand breaks, PARP-1 catalyzes the rapid synthesis of ADP-ribose polymers from the substrate NAD^+, facilitating base excision repair of DNA and signaling to other critical cellular proteins, such as p53 *(2)*. PARP-1 interacts with other components of the base excision repair complex, and cells lacking PARP-1 activity are deficient in base excision repair *(3)*.

PARP-1 inhibitors have potential therapeutic applications *(4)*, including the treatment of cancer *(5)*. Enzyme-mediated DNA repair can cause resistance to DNA-damaging anticancer drugs and radiation, and so inhibition of DNA repair may be therapeutically beneficial *(6)*. PARP-1 activation and subsequent poly-(ADP-ribosylation) are immediate cellular responses to drug- or radiation-induced DNA damage *(2,7)*. Evidence from both inhibitor *(7,8)* and molecular genetic *(9–11)* studies indicates that inhibiting PARP-1-mediated DNA repair increases the cytotoxicity of DNA-damaging cancer therapeutics. However, the therapeutic potential of this approach has not been investigated because of the poor potency, solubility, and limited specificity of classical inhibitors, including 3-substituted benzamides [e.g., 3-aminobenzamide, inhibition constant (K_i) = 5 μ*M;* Fig. 1, A, compound 1 *(12)*] and various fused-ring heterocyclic compounds [Fig. 1, A, compounds 2 and 3 *(13,14)*].

We have developed several inhibitors of PARP-1 with potent chemo- and radiosensitizing activity *in vitro*, including NU1025 (K_i = 50 n*M*, Fig. 1, A, compound 4), that increase the cytotoxicity of the monofunctional DNA-alkylating agent temozolomide, the topoisomerase I inhibitor camptothecin, and γ-irradiation in L1210 cells *(15,16)*. Subsequent studies *(17)* demonstrated that NU1025 and NU1085 (K_i = 6 n*M;* Fig. 1, A, compound 5) increased the activity of temozolomide and the topoisomerase I inhibitor topotecan in 12 human tumor cell lines in a p53-independent manner. However, these compounds still lacked the potency and solubility for extensive preclinical evaluation, although a recent report *(18)* demonstrated that intracranial injection of NU1025 increased the temozolomide-induced survival of mice with brain lymphomas.

Affiliations of authors: Northern Institute for Cancer Research, University of Newcastle upon Tyne, Medical School, Newcastle upon Tyne, U.K. (CRC, SB, MAB, AHC, BWD, SK, DRN, EN, HDT, LZW, NJC); Pfizer Global Research and Development/Agouron Pharmaceuticals, La Jolla, CA (RA, SCK, ZH, RAK, JL, KM, DS, SEW); School of Pharmacy, University of Manchester, Manchester, U.K. (IJS, KJW).

Correspondence to: Nicola J. Curtin, PhD, Northern Institute for Cancer Research, University of Newcastle upon Tyne, Medical School, Framlington Place, Newcastle upon Tyne, NE2 4HH, U.K. (e-mail: n.j.curtin@newcastle.ac.uk).

See "Notes" following "References."

DOI: 10.1093/jnci/djh005

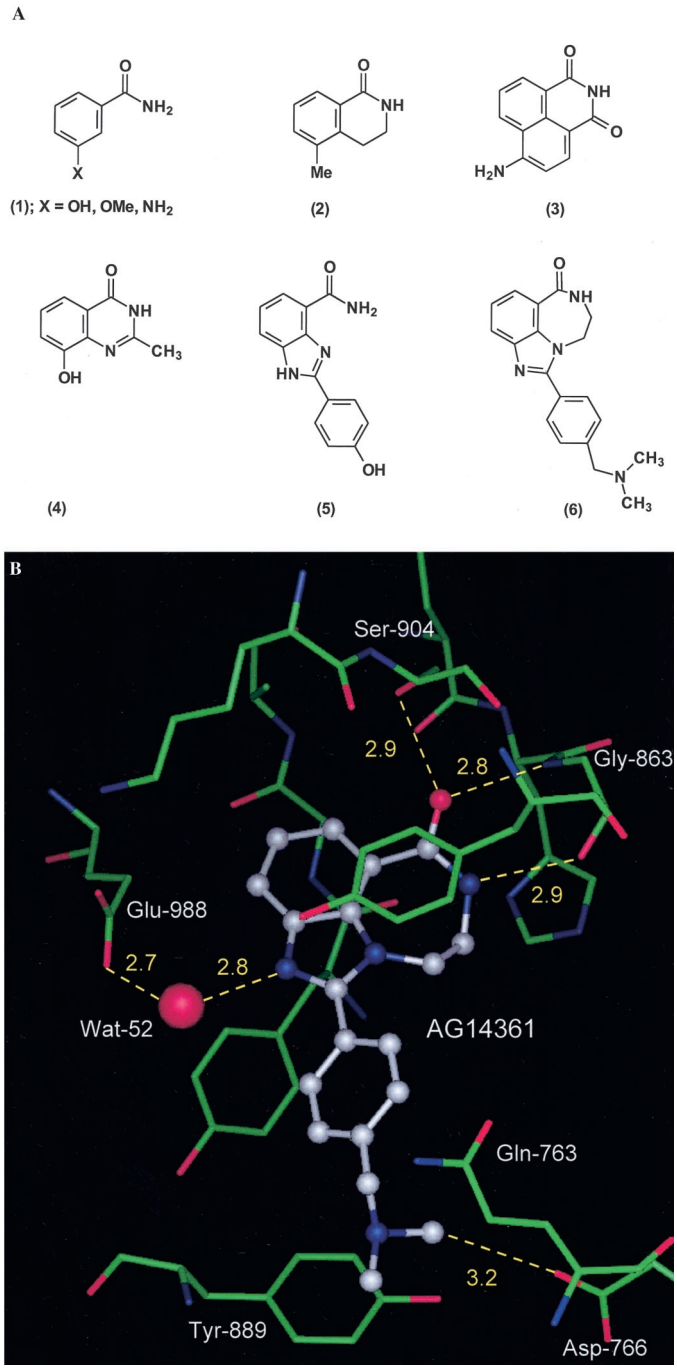

Fig. 1. Inhibitor structures and model of AG14361 in the poly(ADP-ribose) polymerase 1 (PARP-1) catalytic domain. **A**) Chemical structures of selected PARP-1 inhibitors. Compound **1** = substituted benzamides; compounds **2** through **4** = fused-ring heterocyclic compounds; compound **5** = substituted benzimidazole; compound **6** = AG14361. **B**) AG14361 located in the active site of the catalytic domain of chicken PARP-1. AG14361 = **white**; hydrogen bonds = **dotted yellow lines** with the distances (in Å) indicated. Wat = water molecule.

A structural study of NU1085 co-crystallized with the catalytic domain of chicken PARP-1 *(19)* was used to direct the synthesis of additional compounds, with the resulting tricyclic indoles and benzimidazoles being very potent inhibitors of PARP-1 activity. Lead optimization studies *(20)* identified the tricyclic benzimidazole AG14361 (Fig. 1, A, compound 6) as an extremely potent inhibitor (K_i<5 n*M*) that is at least 1000-fold more potent than the benzamides.

The purpose of this study was to determine whether AG14361 increases the effect of anticancer chemotherapy and radiation therapy. We investigated the effects of AG14361 alone and in combination with ionizing radiation, temozolomide, and topoisomerase I poisons in cell culture and in tumor xenograft-bearing mice. These studies were supported by pharmacokinetic (analysis of the metabolic stability of AG14361 *in vitro*, and plasma and tissue concentrations of AG14361 after administration to tumor-bearing mice), pharmacodynamic (measurement of tumor PARP-1 inhibition by AG14361), and mechanistic investigations.

Materials and Methods

Materials

Temozolomide (a gift from the Cancer Research Campaign, London, U.K.), topotecan (SmithKline Beecham Pharmaceuticals, Philadelphia, PA), and AG14361 *(20)* were dissolved in dimethyl sulfoxide to allow addition to cell cultures to a final concentration of 1% dimethyl sulfoxide. For *in vivo* evaluation, drugs were dissolved immediately before administration as follows: temozolomide and irinotecan (Camptosar; Pharmacia Upjohn, Kalamazoo, MI) in normal saline, PD128763 (a gift from Warner-Lambert, Ann Arbor, MI) in 10% dimethyl acetamide in saline, and AG14361 (HCl salt) in saline. Other chemicals and reagents were obtained from Sigma (Poole, U.K.), unless otherwise stated.

Cell Lines and Culture

LoVo and SW620 colorectal cancer cells (American Type Culture Collection, Manassas, VA) and A549 non–small-cell lung carcinoma cells (National Cancer Institute, National Institutes of Health, Bethesda, MD) were maintained in RPMI-1640 medium containing 10% fetal calf serum (Life Technologies, Paisley, U.K.). Mouse embryonic fibroblasts, isolated from PARP-$1^{-/-}$ and PARP-$1^{+/+}$ mice *(11,21)*, were maintained in Dulbecco's modified Eagle medium supplemented with 10% fetal calf serum. Cells were mycoplasma-free *(22)*.

Crystallographic Analysis of AG14361 Bound to the PARP-1 Catalytic Site

Crystals of the catalytic domain of chicken PARP-1 (6 mg/mL) and 200 μ*M* AG14361, added in a 1:1 ratio with 100 m*M* Tris (pH 8.5), 8% 2-propanol, and 16%–30% polyethylene glycol (average molecular weight = 600), were grown at room temperature by the hanging-drop vapor diffusion method *(23)*. X-ray diffraction data, collected at −4 °C, were measured with Cu Kα radiation from a Rigaku rotating anode generator (Rigaku, The Woodlands, TX) and an MAR345 image plate (Mar Research, Evanston, IL). Crystals had a space group of *P*212121, with a = 59.09 Å, b = 64.35 Å, and c = 97.38 Å, and a resolution of 2.15 Å. The structure was solved from a previously determined structure by use of $2|F_{obs}| - |F_{calc}|$ and $|F_{obs}| - |F_{calc}|$ maps and refinement *(24)*, where F_{obs} is the amplitude of the experimentally measured structure factor, and F_{calc} is the amplitude of the structure factor calculated from the model, in this case, a previously determined structure initially

and the current model during refinement. The final *R* factor and *R*-free are 20.1% and 24.4%, respectively, with 0.006 Å and 1.23° root mean square deviations from ideal bond distances and angles, where the *R* factor is the sum of the absolute values of the differences between the observed and calculated structure factor amplitudes divided by the sum of the observed structure factor amplitudes and *R*-free is the *R* factor for a randomly selected subset of reflections that were excluded in the refinement. Molecular modeling of AG14361 with a chimeric human PARP-1 model, created from the co-crystal structure of AG14361 with the catalytic domain of chicken PARP-1 (humanized by changing residue 763 from glutamine to glutamate), used MacroModel version 5.5 *(25)*. Fig. 1, B, was created with Insight II (2000) (Accelrys, San Diego, CA).

PARP-1 Activity Assays

The activity of full-length recombinant human PARP-1 was measured in a reaction mixture containing 20 n*M* PARP-1, 500 μ*M* NAD^+ plus [^{32}P]NAD^+ (0.1–0.3 μCi per reaction mixture; Amersham Pharmacia Biotech, Piscataway, NJ), and activated calf thymus DNA (10 μg/mL) at 25 °C; the reaction was terminated after 4 minutes by adding ice-cold 10% (wt/vol) trichloroacetic acid, as described previously *(26)*. The reaction product [^{32}P]ADP-ribose incorporated into acid-insoluble material was deposited onto Whatman GF/C glass fiber filters with a Bio-Dot microfiltration apparatus (Bio-Rad, Hercules, CA) and quantified with a PhosphorImager (Molecular Dynamics, Sunnyvale, CA). Inhibition of PARP-1 activity by AG14361 at 0–600 n*M* was measured, and the K_i for AG14361 was calculated by nonlinear regression analysis.

We determined PARP-1 inhibition by AG14361 (0–1000 n*M*, *see* Fig. 2, A) in permeabilized cells, as described previously *(27)*, and in intact cells. Briefly, SW620 cells (8×10^5 to 1×10^6 cells per reaction) were permeabilized with digitonin (0.15 mg/mL). PARP-1 activity was stimulated by the addition of 100 ng of 12-mer blunt-ended DNA double-stranded oligonucleotide (2.5 μg/mL) in the presence of 75 μ*M* NAD^+ and [^{32}P]NAD^+ (Amersham) for 6 minutes at 25 °C. Macromolecules were then precipitated with an ice-cold solution of 10% trichloroacetic acid and 10% sodium pyrophosphate, and incorporated radioactivity was measured to determine PARP-1 activity. PARP-1 inhibition was determined by addition of AG14361 (0–1000 n*M*) to the reaction mixture. Intact cells were incubated with AG14361 (1–1000 n*M*, *see* Fig. 2, A) for 10 minutes, rinsed, permeabilized, and assayed for PARP-1 activity as described above. The 50% PARP-1 inhibitory concentration (IC_{50}) for AG14361 was calculated from computer-fitted curves (GraphPad Software, San Diego, CA). PARP-1 activity in tumor homogenates from untreated control and AG14361-treated (10 mg/kg) mice was determined by [^{32}P]NAD^+ incorporation into macromolecules as described for permeabilized cells.

Growth Inhibition and Cytotoxicity Assays *In Vitro*

Cell growth inhibition was estimated in exponentially growing LoVo, A549, and SW620 cells in 96-well plates. Cells were exposed to temozolomide (0–1000 μ*M*, *see* Fig. 4, A) or topotecan (0–30 n*M*, *see* Fig. 4, B) in the presence or absence of 0.4 μ*M* AG14361. Cells were also exposed to AG14361 (0–20 μ*M*, *see* Fig. 4, C) alone or in the presence of 400 μ*M* temozolomide. After 5 days of culture, these cells were fixed with 10% trichloroacetic acid and stained with sulforhodamine B *(28)*. The concentration of temozolomide, topotecan, and AG14361 alone or in combination that inhibited growth by 50% (GI_{50}) was calculated from computer-generated curves. Recovery from potentially lethal damage was measured in confluent LoVo cell cultures arrested in G_1 phase (confirmed by flow cytometry, data not shown) to mimic the radiation-resistant quiescent cell population in tumors. Such cells were exposed to 8 Gy of γ-irradiation (Gammacell 1000 Elite; Nordion International, Kanata, Ontario, Canada) and then harvested and plated for colony formation assay immediately or maintained as growth-arrested confluent cultures for a 4-hour or 24-hour recovery period before harvesting and plating for the colony formation assay. Where indicated, 0.4 μ*M* AG14361 was added 30 minutes before irradiation and was present in the recovery incubation.

Microarray Analysis

Changes in gene expression after exposure to AG14361 (0.4 μ*M* or 14 μ*M*) were determined by use of RNA extracted from A549 cells with TRIzol (GIBCO/BRL Invitrogen, Carlsbad, CA) and the RNeasy mini-column (Qiagen, Valencia, CA), according to the manufacturers' instructions. RNA was hybridized on human Hu6800 high-density oligonucleotide arrays (Affymetrix, Santa Clara, CA), as previously described *(29,30)*. Analysis of the arrays by GeneChip 3.2 (Affymetrix) scaled to an average hybridization intensity of 200 is estimated to represent three to five copies per cell, and an expression ratio of twofold is the approximate limit of sensitivity *(31)*.

AG14361 Metabolic Stability and Plasma and Tissue Distribution

The *in vitro* metabolic stability of AG14361 was determined in microsomal preparations (prepared by differential centrifugation of homogenized frozen liver tissue) from mouse, rat, dog, monkey, and human liver. AG14361 (5 μ*M*) was incubated with microsomal preparations (0.5 mg of protein per mL) and an NADPH-generating system (glucose-6-phosphate, glucose-6-phosphate dehydrogenase, and NADP) at 37 °C for 0.5 and 2 hours. The concentration of AG14361 remaining was determined by high-performance liquid chromatography–mass spectrometry/mass spectrometry (HPLC–MS/MS) (HP 1100DAD; Hewlett-Packard; mobile-phase and gradient 5%–61% acetonitrile in 0.1% formic acid with a Zorbax Eclipse C18 column, 2.1 × 50 mm) coupled to a Quattro II triple quadrupole mass spectrometer (Micromass). The initial and remaining concentrations of AG14361 were compared to determine its molecular stability.

The plasma concentration and tissue distribution of AG14361 was determined 30, 60, and 120 minutes (*see* Fig. 3, B) after intraperitoneal administration to CD-1 nude mice (Charles River, Margate, U.K.) bearing subcutaneous LoVo or SW620 xenografts (approximately 650 mm^3). The concentration of AG14361 in acetonitrile-treated plasma and homogenized tissues was measured with reversed-phase HPLC (isocratic mobile phase = 40% acetonitrile in 0.1% ammonium formate; Hypersil BDS column of 4.6 × 250 mm and 5-μm particle size; Waters Alliance 2780 HPLC) by the method of addition *(32)*. Animal care was in accordance with institutional guidelines.

Acute Toxicity of AG14361 in PARP-$1^{+/+}$ and PARP-$1^{-/-}$ Mice

Female PARP-$1^{+/+}$ and PARP-$1^{-/-}$ mice, three mice per group [supplied by J. Menissier-de Murcia and G. de Murcia *(11)*], were treated with PD128763 or AG14361 (each at 50 mg/kg, intraperitoneally), and the effect on body temperature (an indicator of acute hypotension) was measured for up to 10 hours after treatment with a Testo 925 electronic rectal thermometer (Testo, Alton, U.K.).

Tumor Growth Inhibition

CD-1 nude mice bearing palpable, subcutaneous SW620 or LoVo xenografts were treated intraperitoneally with normal saline (control animals) or AG14361 (at 5 or 15 mg/kg) alone daily for 5 days (five mice per group). For drug combinations, AG14361 was administered intraperitoneally daily for 5 days immediately before administering the cytotoxic drug (temozolomide at 68 mg/kg orally or irinotecan at 2.5 mg/kg intraperitoneally) or 30 minutes before applying 2 Gy of x-irradiation locally to the tumor daily for 5 days. Tumor volumes, determined from two-dimensional caliper measurements and the equation $a^2 \times b/2$ (where a is the width and b is the length of the tumor), are presented as median relative tumor volume (RTV). That is, RTV1 is the tumor volume on the initial day of treatment (day 0), and RTV4 is the tumor volume 4 times that on the initial day of treatment. Tumor growth delay is defined as the time to RTV4 in drug-treated or irradiated mice compared with the time to RTV4 in control (vehicle alone) mice.

Median tumor volume is shown, rather than the mean, as this is generally accepted as the most statistically reliable representation of the average growth rate of tumors in a small group of mice, where a normal distribution of tumor volumes cannot be assumed. RTV4 was chosen as the most robust measurement that does not result in unacceptable suffering for the animals.

Tumor Perfusion Assay

AG14361 (10 mg/kg) or saline (control) was administered intraperitoneally to mice bearing SW620 xenografts 30 minutes before intravenous injection of Hoechst 33342 dye (15 mg/kg, dissolved in phosphate-buffered saline), followed 20 minutes later by the administration of carbocyanine (1 mg/kg, dissolved in 75% dimethyl sulfoxide); 5 minutes later, tumors were excised and frozen as described previously *(33)*. To measure stained vessels, tumor sections (10 μm) were scanned under a Nikon Eclipse E800 microscope (excitation wavelengths = 340–380 nm and 450–490 nm; emission wavelengths = 480 nm and 510 nm, for Hoechst and carbocyanine, respectively) to determine the percentage of Hoechst- and carbocyanine-positive vessels.

Statistical Analysis

Cell growth inhibition and cytotoxicity assays were analyzed with paired or unpaired Student's *t* tests when the variances were equal or with Wilcoxon rank tests or Mann–Whitney *U* tests, as appropriate. RTVs and tumor perfusion values were compared with the Mann–Whitney *U* test. All statistical tests were two-sided.

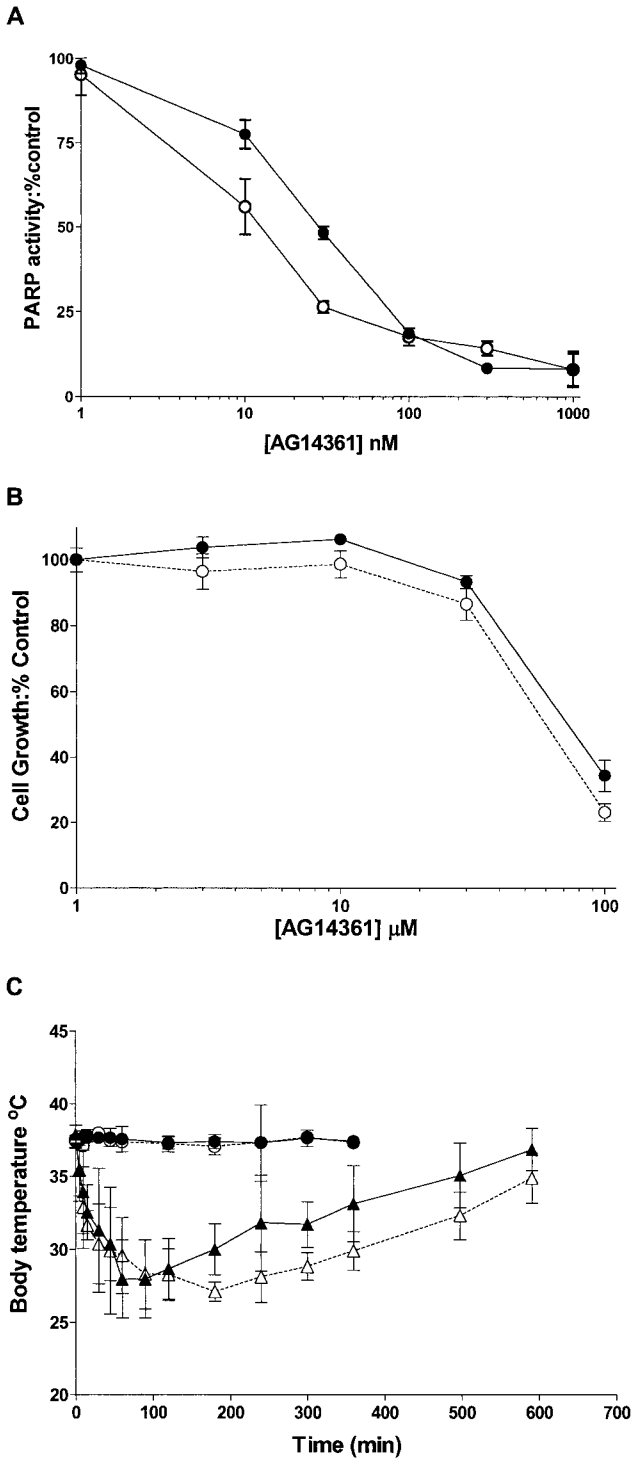

Fig. 2. Effect of AG14361 on cellular poly(ADP-ribose) polymerase 1 (PARP-1) activity, cell proliferation, and body temperature in mice. **A**) Inhibition of PARP-1 activity in permeabilized (**solid circles**) and intact (**open circles**) SW620 cells. Data are the mean of pooled data from two experiments, each one with triplicate measurements at each concentration. **B**) Cell growth inhibition induced by AG14361 in PARP-$1^{-/-}$ (**open circles**) and PARP-$1^{+/+}$ (**solid circles**) mouse embryonic fibroblasts. Data are from a single representative experiment (others were similar) with six replicates at each concentration. **C**) Changes in body temperature of mice after intraperitoneal administration of another PARP-1 inhibitor PD128763 at 50 mg/kg (**solid** and **open triangles**) or AG14361 at 50 mg/kg (**solid** and **open circles**) to female PARP-$1^{+/+}$ (**solid triangles** and **circles**) and PARP-$1^{-/-}$ (**open triangles** and **circles**) mice. Data are the mean of three mice per group. **A–C**) **Error bars** represent 95% confidence intervals.

RESULTS

Interaction of AG14361 With the Active Site of PARP-1

Crystallographic analysis of AG14361 bound to the catalytic domain of chicken PARP-1 (Fig. 1, B) showed that the tricyclic ring system of AG14361 was located in a pocket composed of amino acid residues Trp861, His862, Gly863, Tyr896, Phe897, Ala898, Lys903, Ser904, Tyr907, and Glu988. The 2-phenyl group extended outward and was exposed to bulk solvent on both faces; the 4′-dimethylaminomethyl moiety resided in a pocket composed of residues Gln759, Val762, Gln763, Asp766, Gly888, and Tyr889. AG14361 formed important hydrogen bonds with Ser904 and Gly863 and a water-mediated hydrogen bond with Glu988. The 4′-dimethylaminomethyl group formed an ion pair with Asp766 through a hydrogen bond between C-H and O and participated in a cation--π interaction with Tyr889. In human PARP-1, residue 763 is glutamate, which can form an additional ionic interaction with the 4′-dimethylaminomethyl group.

AG14361 and PARP-1 Inhibition *In Vitro* and in Whole Cells

AG14361 is a potent inhibitor of purified full-length human PARP-1 [K_i<5 n*M;* the limit of accurate kinetic determination for this homodimeric enzyme *(34)*]. The IC_{50} for AG14361 was 29 n*M* in permeabilized SW620 cells and 14 n*M* in intact SW620 cells (Fig. 2, A). To investigate whether AG14361 increased the effect of chemotherapeutic agents or radiation therapy, we used 0.4 μ*M* AG14361, a concentration that inhibited PARP-1 activity by more than 85%.

Specificity of AG14361 for PARP-1 *In Vitro* and *In Vivo*

The specificity of AG14361 for PARP-1 was determined by investigating the effect of AG14361 on gene expression and cellular proliferation of human cancer cells and by investigating whether any growth-inhibitory effect or acute toxicity of AG14361 was related to PARP-1 in PARP-$1^{-/-}$ cells and mice compared with their wild-type counterparts. The GI_{50} of AG14361 alone (a 5-day continuous exposure) was 14 μ*M* (95% confidence interval [CI] = 9 to 19 μ*M*), 11.2 μ*M* (95% CI = 8 to 14.4 μ*M*), and more than 20 μ*M* in cultured A549, LoVo, and SW620 cells, respectively. AG14361-induced growth inhibition was not attributed to PARP-1-related effects because maximal PARP-1 inhibition was observed at much lower concentrations (≤1 μ*M;* Fig. 2, A) than the GI_{50}. We observed identical levels of AG14361-induced growth inhibition in cell lines derived from PARP-$1^{-/-}$ and PARP-$1^{+/+}$ mice (mean GI_{50} = 66 and 65 μ*M*, respectively; Fig. 2, B). In addition, 0.4 μ*M* AG14361 did not substantially alter gene expression as shown by microarray analysis. A 17-hour exposure of A549 cells to 0.4 μ*M* AG14361 did not change the expression of the 6800 genes studied by more than twofold. Changes of more than twofold were observed in the expression of 62 of these genes, including p21, at the GI_{50} of AG14361 (data not shown). Thus, although 0.4 μ*M* AG14361 inhibited cellular PARP-1 activity by more than 85%, it essentially did not change gene expression and cell proliferation, indicating that the cellular effects of this low concentration of AG14361 are specific for PARP-1 inhibition. Higher, growth-inhibitory concentrations of AG14361 did affect gene expression, but these effects are not likely to be related to PARP-1

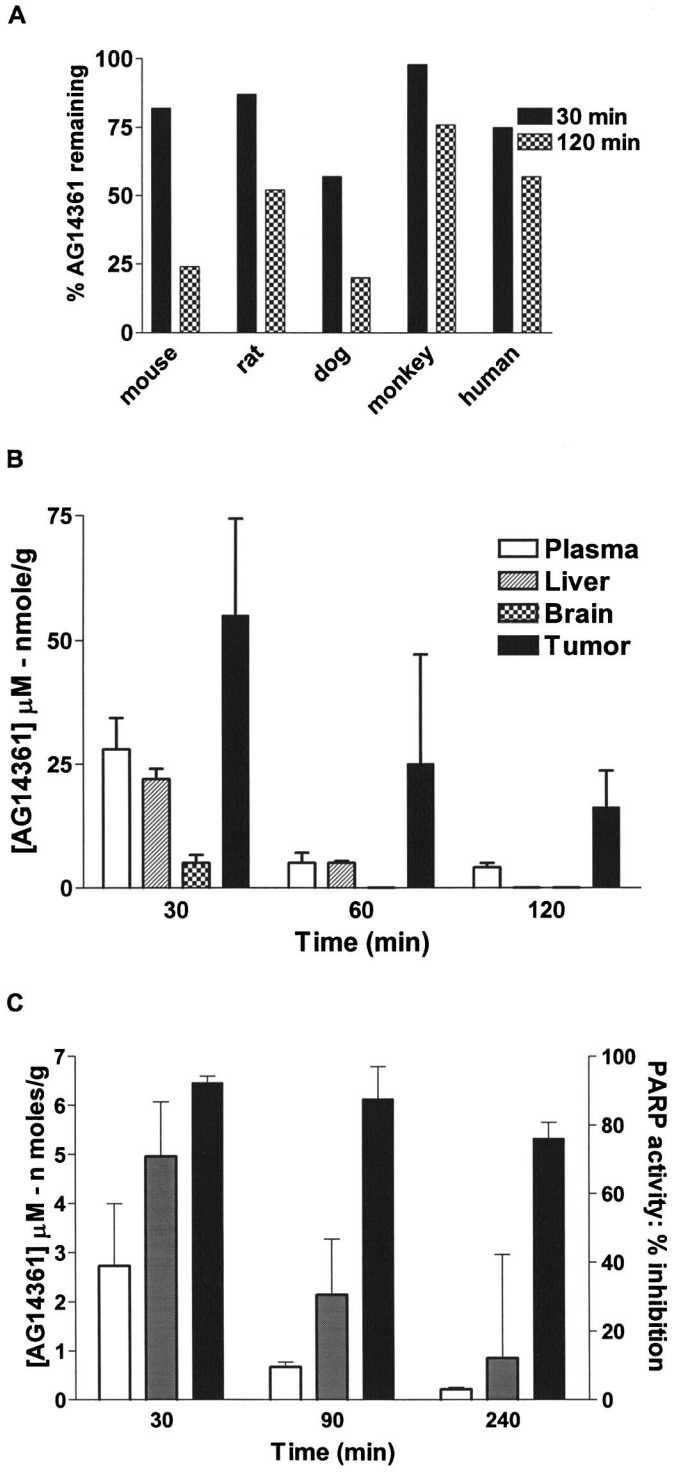

Fig. 3. AG14361 metabolic stability, tissue distribution, and tumor poly(ADP-ribose) polymerase 1 (PARP-1) inhibition. **A**) Metabolic stability of AG14361 (initial concentration = 5 μ*M*) after 30-minute and 120-minute incubations with hepatic microsomal preparations from the indicated mammalian species. Data are the means of duplicate measurements. **B**) Plasma pharmacokinetics and distribution of AG14361 in the plasma, liver, brain, and LoVo xenograft tumors after intraperitoneal administration of AG14361 at 50 mg/kg at the indicated times. Data are the mean from three tumor-bearing animals. **C**) Concentrations of AG14361 in plasma (**open bars**) and SW620 xenograft tumors (**shaded bars**) and inhibition of PARP-1 activity in SW620 xenograft tumor homogenates (**solid bars**) after intraperitoneal administration of AG14361 at 10 mg/kg. Data are the mean from three tumor-bearing animals. The right *y*-axis shows inhibition of PARP-1 activity; the left *y*-axis shows the concentration of AG14361 in plasma and tumor tissue. **B** and **C**) Error bars represent 95% confidence intervals.

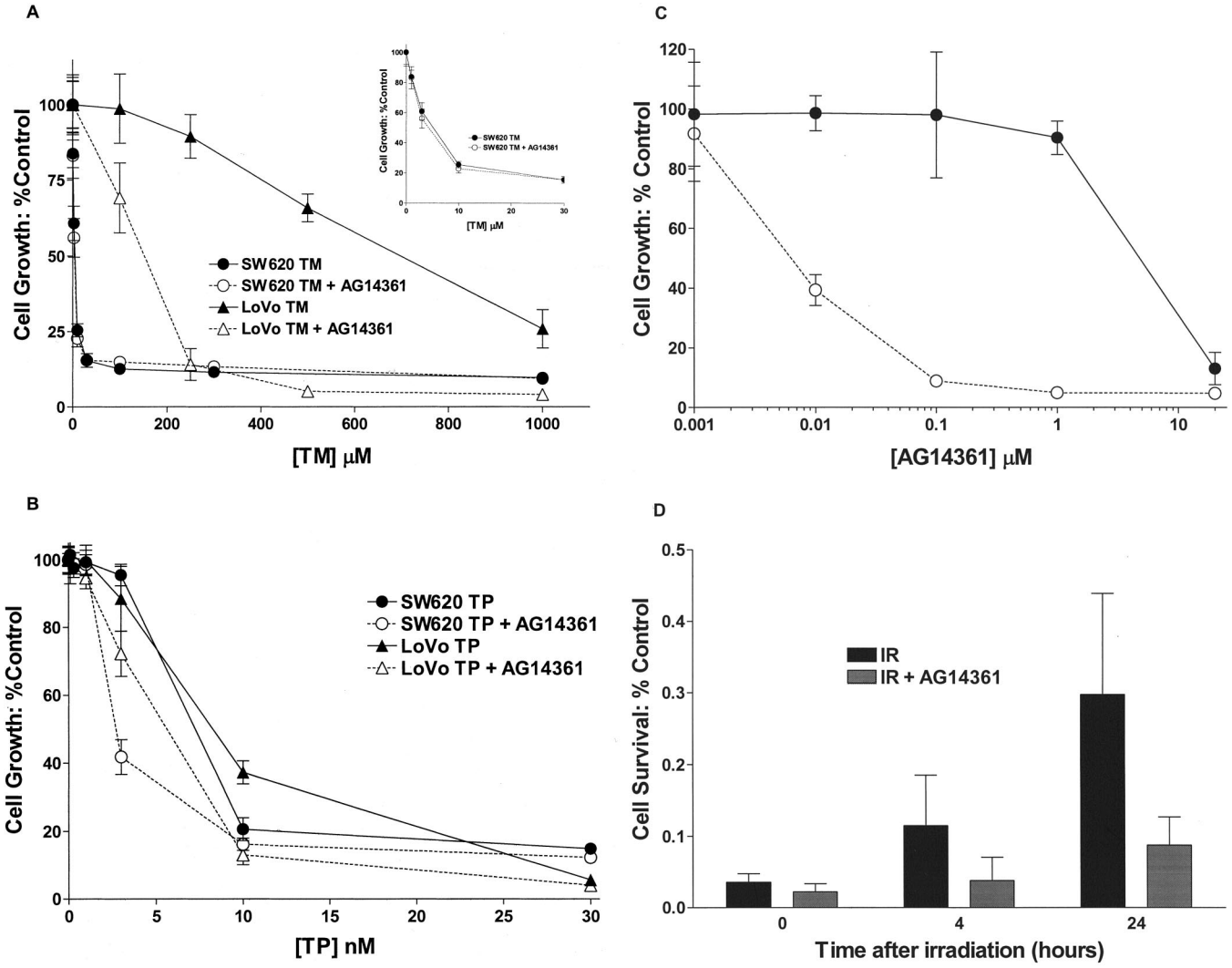

Fig. 4. Enhancement of chemotherapy and radiation therapy *in vitro* by AG14361. **A**) Cell growth inhibition was determined after a 5-day exposure to temozolomide (TM) alone (**solid triangles** and **circles**) or with 0.4 μ*M* AG14361 (**open triangles** and **circles**). LoVo cells = **solid** and **open triangles**; SW620 cells = **solid** and **open circles**. Data are the mean of six replicates (normalized to 1% dimethyl sulfoxide or 0.4 μ*M* AG14361-alone control, as appropriate) from a single representative experiment; data from others were similar. Inset shows the data for SW620 cells exposed to 0–30 μ*M* TM with or without 0.4 μ*M* AG14361. **B**) Cell growth inhibition was determined after a 5-day exposure to topotecan (TP) alone (**solid triangles** and **circles**) or with 0.4 μ*M* AG14361 (**open triangles** and **circles**). LoVo cells = **solid** and **open triangles**; SW620 cells = **solid** and **open circles**. Data are the mean of six replicates (normalized to 1% dimethyl sulfoxide or 0.4 μ*M* AG14361-alone control, as appropriate) from a single representative experiment. **C**) Growth inhibition of LoVo cells was determined after a 5-day exposure to AG14361 alone (**solid circles**) or with 400 μ*M* TM (**open circles**). Data are the mean of six replicates (normalized to 1% dimethyl sulfoxide or 400 μ*M* TM-alone control, as appropriate) from a single representative experiment in which the 50% growth inhibitory concentration (GI_{50}) for AG14361 alone was 10.9 μ*M* and the GI_{50} for AG14361 plus TM was 0.007 μ*M*. **D**) Recovery from potentially lethal damage induced by 8 Gy of γ-irradiation of confluent LoVo cells arrested in G_1 phase. Cells were seeded immediately (0 hour) or after 4 or 24 hours of recovery in control medium (**solid bars**) or medium containing 0.4 μ*M* AG14361 (**shaded bars**). Data are the mean of three independent experiments (three replicates from each experiment). **A–D**) **Error bars** represent 95% confidence intervals.

inhibition because cell proliferation was affected equally in $PARP^{-/-}$ and $PARP\text{-}1^{+/+}$ cells.

Acute hypotension and hypothermia have been reported in mice treated with the PARP-1 inhibitor PD128763 (Fig. 1, A, compound 2) at doses that increased the antitumor activity of radiation therapy *(35)*. To determine whether this result was caused by PARP-1 inhibition and whether AG14361, therefore, would have a similar side effect, we treated $PARP\text{-}1^{-/-}$ and $PARP\text{-}1^{+/+}$ mice (three per group) with such doses (50 mg/kg) of PD128763 and AG14361 and evaluated their effect on mouse body temperature, an indicator of acute hypotension. Although PD128763 caused profound hypothermia in $PARP\text{-}1^{+/+}$ mice (nadir = 28 °C, 95% CI = 27 to 29 °C) and $PARP\text{-}1^{-/-}$ mice (nadir = 27.1 °C, 95% CI = 26.7 to 27.3 °C) compared with control mice (temperature = 37.5 °C, 95% CI = 37.4 to 37.6 °C), AG14361 did not affect mouse body temperature in $PARP\text{-}1^{+/+}$ (mean temperature = 37.4 °C, 95% CI = 37.2 to 37.6 °C) or $PARP\text{-}1^{-/-}$ mice (mean temperature = 37.4 °C, 95% CI = 37.3 to 37.5 °C) (Fig. 2, C). Because the more potent PARP-1 inhibitor AG14361 did not induce hypothermia and because PD128763-induced hypothermia was similar in $PARP\text{-}1^{-/-}$ and $PARP\text{-}1^{+/+}$ mice, hypothermia apparently did not result from PARP-1 inhibition.

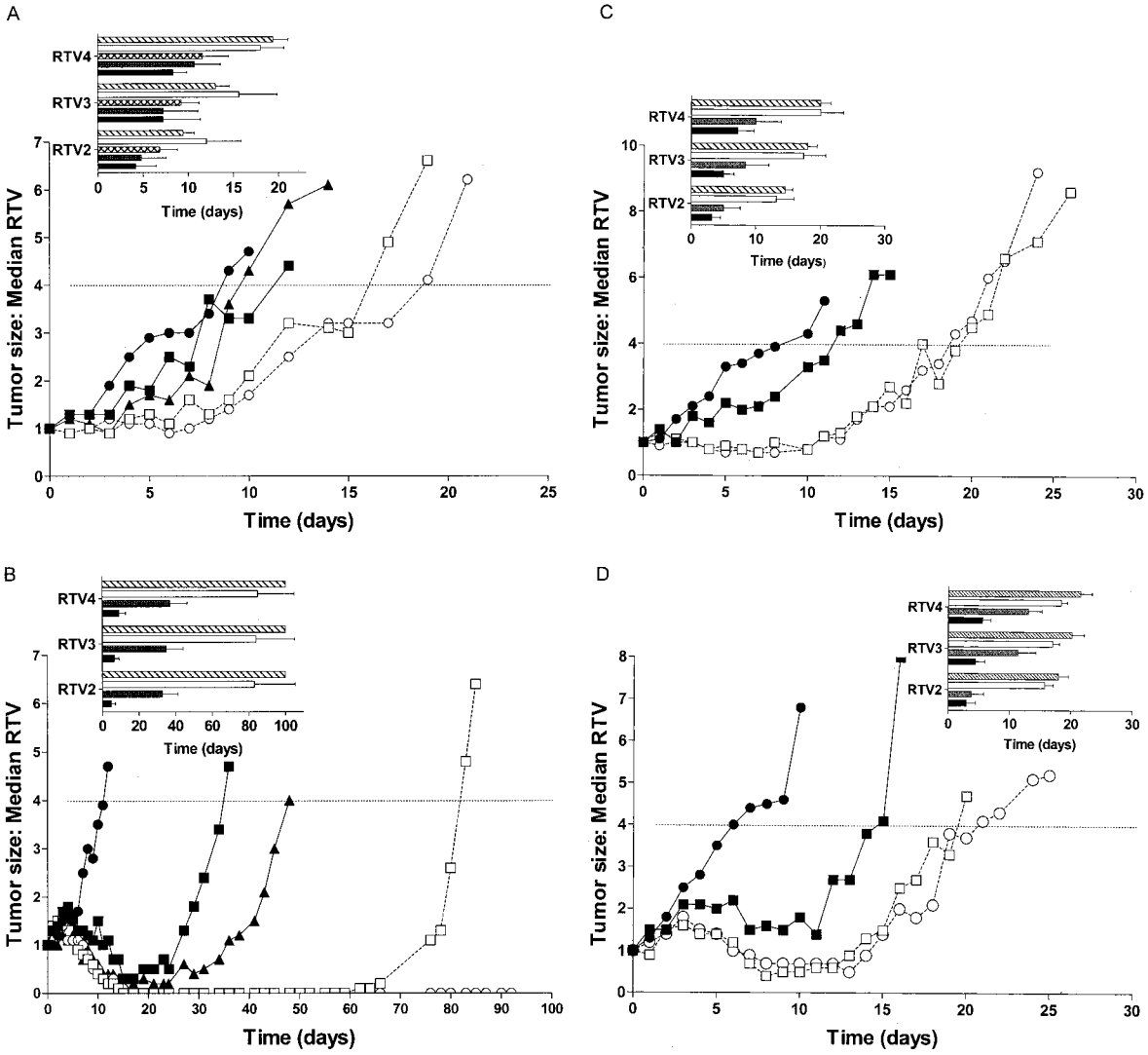

Fig. 5. Enhancement of antitumor chemotherapy and radiation therapy by AG14361 in tumor-bearing mice. For all experiments, tumor growth is presented as the median relative tumor volume (RTV; five animals per group). Insets represent time taken (days) for tumors to reach RTV2, RTV3, and RTV4 (mean ± 95% confidence interval). **A**) Growth of LoVo tumor xenografts after daily treatment for 5 days with vehicle control alone (**solid circles, solid bars**), temozolomide (TM) at 68 mg/kg (**solid squares, shaded bars**), TM at 136 mg/kg (**solid triangles, cross-hatched bars**), TM at 68 mg/kg + AG14361 at 5 mg/kg (**open squares, open bars**), or TM at 68 mg/kg + AG14361 at 15 mg/kg (**open circles, hatched bars**). **B**) Growth of SW620 tumor xenografts after daily treatment for 5 days with vehicle control alone (**solid circles, solid bars**), TM at 68 mg/kg (**solid squares, shaded bars**), TM at 136 mg/kg (**solid triangles**), TM at 68 mg/kg + AG14361 at 5 mg/kg (**open squares, open bars**), or TM at 68 mg/kg + AG14361 at 15 mg/kg (**open circles, hatched bars**). **C**) Growth of LoVo tumor xenografts after daily treatment for 5 days with vehicle control alone (**solid circles, solid bars**), irinotecan (Irino) at 2.5 mg/kg (**solid squares, shaded bars**), Irino at 2.5 mg/kg + AG14361 at 5 mg/kg (**open squares, open bars**), or Irino at 2.5 mg/kg + AG14361 at 15 mg/kg (**open circles, hatched bars**). **D**) Growth of SW620 tumor xenografts after daily treatment for 5 days with vehicle control alone (**solid circles, solid bars**), Irino at 2.5 mg/kg (**solid squares, shaded bars**), Irino at 2.5 mg/kg + AG14361 at 5 mg/kg (**open squares, open bars**), or Irino at 2.5 mg/kg + AG14361 at 15 mg/kg (**open circles, hatched bars**). **(Continued on facing page).**

Metabolic Stability of AG14361, Tissue Distribution, and Tumor PARP-1 Inhibition

The metabolic stability of AG14361 (5 μ*M*) was tested *in vitro* in liver microsomal preparations from mice, rats, dogs, monkeys, and humans (Fig. 3, A). After a 2-hour incubation with such microsomal preparations, at least 50% of the initial concentration of AG14361 remained with the human preparations, but only 25% remained with the murine preparations.

Plasma and tissue distribution studies in mice bearing LoVo (Fig. 3, B) and SW620 (data not shown) xenografts after intraperitoneal administration of AG14361 at 50 mg/kg demonstrated that AG14361 was rapidly absorbed into the bloodstream and distributed to the tumor and liver with lower concentrations detected in the brain. Tissue-to-plasma concentration ratios indicated that AG14361 was retained in tumor tissue over time in both xenograft models, with tumor concentrations (≥15 μ*M* for 2 hours) in excess of that required to inhibit PARP-1 activity *in vitro.*

PARP-1 activity, detected by pharmacodynamic assay, in SW620 xenografts was inhibited by more than 75% for at least 4 hours after intraperitoneal administration of AG14361 (10 mg/kg), consistent with the concentration of AG14361 persisting in the tumor (Fig. 3, C). Inhibition of PARP-1 activity was confirmed at doses that increase the effect of chemotherapeutic

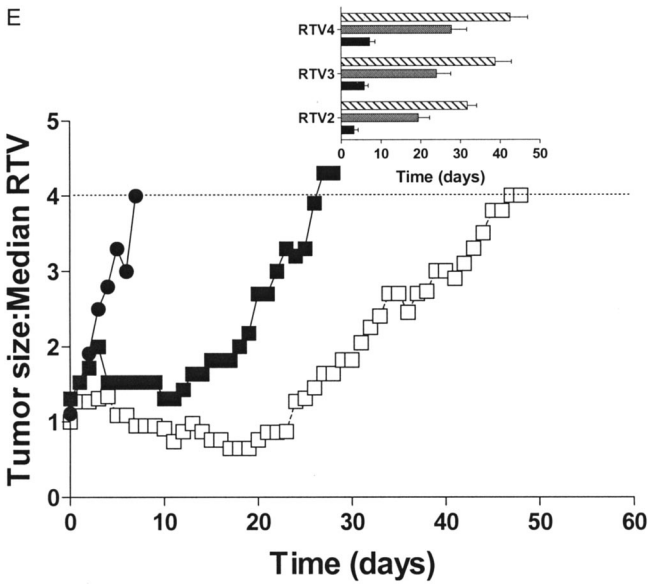

Fig. 5. (Continued from facing page). E) Growth of SW620 tumor xenografts after daily treatment for 5 days with vehicle control alone (**solid circles, solid bars**), 2 Gy of x-irradiation (IR) + vehicle (**solid squares, shaded bars**), or 2 Gy of x-irradiation + AG14361 at 15 mg/kg (**open squares, hatched bars**).

agents and radiation therapy. At 30 minutes after intraperitoneal administration, AG14361 at 5 mg/kg inhibited PARP-1 activity by 75% (95% CI = 67% to 83%) and AG14361 at 15 mg/kg inhibited PARP-1 activity by 90% (95% CI = 89% to 91%).

Combination of Chemotherapy or Radiation Therapy With AG14361 in Cultured Human Cancer Cells

The effect of 0.4 μM AG14361 (>100 times the K_i and <5% of the GI_{50} values) on temozolomide- and topotecan-induced growth inhibition was measured in A549, LoVo, and SW620 cell cultures (Fig. 4, A and B). In combination with temozolomide, AG14361 statistically significantly reduced the temozolomide GI_{50} value 5.5-fold (95% CI = 4.9-fold to 5.9-fold; P = .004) in LoVo cells and reduced the GI_{50} value 2.1-fold or 2.3-fold (in two independent experiments) in A549 cells, but AG14361 failed to reduce the temozolomide GI_{50} value in SW620 cells. In combination with topotecan, AG14361 statistically significantly reduced the topotecan GI_{50} value 1.7-fold (95% CI = 1.3-fold to 2.1-fold; P = .020) in SW620 cells, 1.6-fold (95% CI = 1.3-fold to 1.9-fold; P = .002) in LoVo cells, and 1.9-fold or 2.1-fold (two independent experiments) in A549 cells. Growth inhibition of LoVo cells by AG14361 alone or in combination with 400 μM temozolomide (approximately half its GI_{50} concentration; temozolomide GI_{50} = 789 μM, 95% CI = 713 to 865 μM) demonstrated that concentrations in excess of 1.0 μM AG14361 alone were required to retard cell growth, whereas only 0.1 μM AG14361 was required for the maximum potentiation of temozolomide (Fig. 4, C).

A contributory factor to radiation resistance *in vivo* is the ability of quiescent cells to repair potentially lethal damage *(36)*. In *in vitro* models of recovery from potentially lethal irradiation damage, the increased survival of growth-arrested cells is assessed by colony formation assay after a recovery period and compared with that of cells without the recovery period. Confluent LoVo cells, arrested in G_1 phase, were exposed to 8 Gy of irradiation and then replated to assess their colony-forming ability immediately after irradiation or after a 4- or 24-hour recovery incubation in control medium or medium containing 0.4 μM AG14361 (Fig. 4, D). Survival increased approximately sevenfold for cells given a 24-hour recovery period in control medium before replating for the colony-forming assay compared with that of cells replated for colony formation immediately after irradiation. The increase in survival of cells exposed to AG14361 during the recovery period was statistically significantly reduced (P = .002) compared with that of cells not treated with AG14361, such that AG14361 inhibited the recovery of cells by 73% (95% CI = 48% to 98%) at 24 hours.

Combination of Chemotherapy or Radiation Therapy With AG14361 in Human Tumor Xenografts

The effect of AG14361 on the antitumor activity of temozolomide, irinotecan, and x-irradiation was determined in mice bearing established subcutaneous human LoVo or SW620 tumor xenografts (five mice per treatment group). At the doses used (5 and 15 mg/kg), AG14361 alone did not induce toxicity or affect tumor growth. Temozolomide alone at 68 mg/kg given daily for 5 days [approximately equivalent to the recommended schedule in patients of 200 mg/m^2 per day *(37)*] induced a tumor growth delay (time to RTV4) of 3 days (95% CI = 0 to 6 days) for LoVo xenografts and 24 days (95% CI = 16 to 32 days) for SW620 xenografts (Fig. 5, A and B). Increasing the temozolomide dose to 136 mg/kg (Fig. 5, A and B) or increasing the duration of administration to 68 mg/kg given daily for 10 days (data not shown) did not markedly augment its activity. In contrast, coadministration of AG14361 with temozolomide statistically significantly increased temozolomide activity against LoVo xenografts, with the tumor growth delay being increased from 3 days to 9 days (95% CI = 7 to 11 days; P = .032) by AG14361 at 5 mg/kg and to 10 days (95% CI = 8 to 12 days; P = .032) by AG14361 at 15 mg/kg (Fig. 5, A). This effect on temozolomide activity was even more pronounced in mice bearing SW620 xenografts, with a 100% complete remission rate observed with temozolomide and AG14361, an effect that persisted for 60 days in mice receiving temozolomide at 68 mg/kg plus AG14361 at 5 mg/kg or until 100 days in mice receiving temozolomide at 68 mg/kg plus AG14361 at 15 mg/kg, when mice were killed (Fig. 5, B). Limited toxicity, reflected by loss of body weight, was observed in mice treated with temozolomide alone at 68 mg/kg (nadir body weight = 92% of initial weight, 95% CI = 85% to 99%), which was not statistically significant (P = .310); this value was not statistically significantly increased by AG14361 at 5 mg/kg (nadir body weight = 93% of initial weight, 95% CI = 88% to 98%). However, statistically significant loss of body weight was observed in mice treated with temozolomide at 138 mg/kg (nadir = 88% of initial weight, 95% CI = 84% to 92%; P = .032) and the combination of AG14361 at 15 mg/kg and temozolomide at 68 mg/kg (nadir = 80% of initial weight, 95% CI = 71% to 88%; P = .016), including one toxic death.

In mice bearing LoVo xenografts, irinotecan (2.5 mg/kg given daily for 5 days intraperitoneally) delayed xenograft tumor growth by 4 days (95% CI = 2 to 7 days). When AG14361 at 5 or 15 mg/kg was administered with irinotecan, the growth delay was statistically significantly increased to 9 days (95%

CI = 7 to 11 days; $P = .016$) or to 11 days (95% CI = 9 to 13 days; $P = .008$), respectively (Fig. 5, C). Similarly, in mice bearing SW620 xenografts, irinotecan alone delayed xenograft tumor growth 8 days (95% CI = 6 to 10 days). When AG14361 at 5 or 15 mg/kg was administered with irinotecan, the delay was statistically significantly increased to 14 days (95% CI = 12 to 16 days; $P = .001$) or 16 days (95% CI = 15 to 17 days; $P = .002$), respectively (Fig. 5, D). No statistically significant loss of body weight was observed in the single-agent irinotecan groups, and only limited loss of body weight was observed in the irinotecan combination groups (nadir body weight in the high-dose combination group = 91% of initial weight, 95% CI = 86% to 96%; $P = .69$). Diarrhea, the normal indicator of gastrointestinal tract toxicity associated with irinotecan, was not observed in these animals.

AG14361 treatment before irradiation statistically significantly increased the sensitivity to radiation therapy of mice bearing LoVo xenografts ($P = .008$). Local tumor irradiation (2 Gy daily for 5 days) alone caused a 19-day tumor growth delay (95% CI = 16 to 22 days) that was extended to a 37-day delay (95% CI = 35 to 39 days) in mice treated with AG14361 at 15 mg/kg before irradiation (Fig. 5, E). Local toxicity in normal tissues was not observed in either group.

The increased antitumor activity observed with the combination of temozolomide and AG14361 in SW620 xenografts (Fig. 5, B) was not predicted from the *in vitro* data (Fig. 4, A). Consequently, we investigated whether AG14361 has vasoactive properties, as observed with nicotinamide (a weak PARP-1 inhibitor) and other benzamide analogs *(38)*. Fluorescent markers of vascular perfusion detected a "mismatch" (lack of overlap) of vessels stained with both dyes (resulting from intermittent blood flow) in control SW620 tumors that was statistically significantly reduced by pretreatment with AG14361 ($P = .022$) (Fig. 6). Blood flow was maintained in 88% (95% CI = 78% to 98%) of the Hoechst-stained vessels in the AG14361-treated group but was maintained in 58% (95% CI = 31% to 84%) of those in the control tumors (seven tumors per group). AG14361 therefore statistically significantly increased blood flow in xenografts and thus potentially increased drug delivery to tumor xenografts.

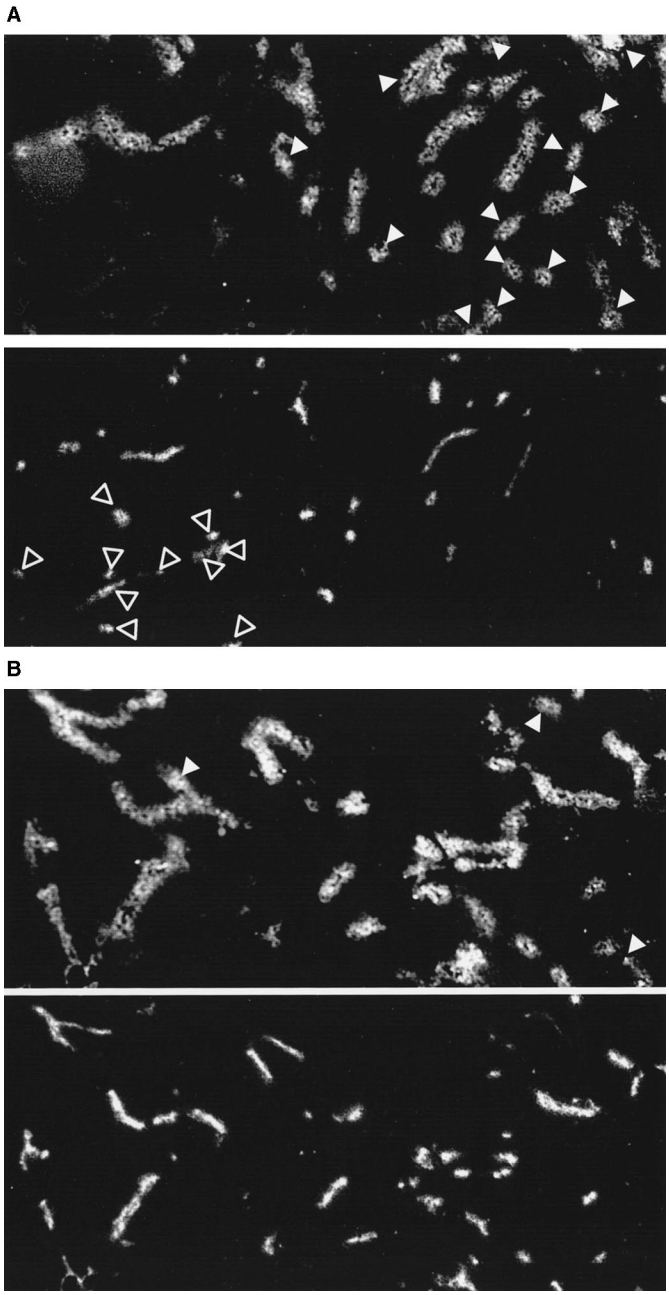

Fig. 6. Effect of AG14361 on tumor vasculature. Two perfusion markers, Hoechst (**upper panels**) and carbocyanine (**lower panels**), were administered with a 20-minute interval between treatments to mice bearing SW620 xenografts treated with saline (**A**) or AG14361 (**B**). **Solid arrowheads** = vessels that were open only at the time of Hoechst administration; **open arrowheads** = vessels that were open only at the time of carbocyanine administration. Pretreatment with AG14361, compared with pretreatment with saline, markedly reduced the number of vessels subjected to intermittent flow in the interval between the addition of the two markers (indicated by **arrowheads**).

DISCUSSION

The implications of DNA repair inhibitors for anticancer therapy are well recognized *(39)*, and the role of PARP-1 in DNA damage repair has been extensively characterized. First-generation PARP-1 inhibitors, such as 3-aminobenzamide, lacked the potency, specificity, and pharmacologic properties required for detailed preclinical evaluation of their ability to increase the sensitivity of tumors to anticancer chemotherapy and radiation therapy *(5,6)*. Although researchers in a limited number of *in vivo* anticancer studies of second-generation PARP-1 inhibitors in combination with cytotoxic agents have observed increased survival compared with chemotherapy alone *(4,18,40)*, most *in vivo* investigations of second-generation PARP-1 inhibitors have focused on protecting normal tissue from oxidative damage by using a variety of models of human pathophysiologic states [for review, *see (41)*].

AG14361 is more than 1000 times more potent than 3-aminobenzamide *(20)*, and x-ray crystallographic analysis shows that AG14361 makes several critical interactions within the active site of PARP-1. AG14361 at 0.4 μM inhibited PARP-1 activity by more than 85% without affecting gene expression or cell proliferation (Fig. 2). At this low concentration, AG14361 increased the activity of DNA-damaging chemotherapeutic agents, temozolomide and topotecan, and the activity of radiation therapy *in vitro* (Fig. 4). AG14361 at this concentration also inhibited the recovery of growth-arrested cells from

potentially lethal irradiation damage by approximately 75% (Fig. 4, D). This sensitization of growth-arrested cells is important for tumor radiation therapy because experimental and clinical evidence indicate that the growth-arrested cell fraction within a tumor is radiation-resistant and capable of re-entering the cell proliferation cycle and thereby re-populating the tumor after radiation therapy *(36,42)*.

Pharmacologic studies demonstrated limited metabolic degradation of AG14361 by human liver microsomes *in vitro*, the retention of AG14361 in the tumor, and the inhibition of tumor PARP-1 activity by 75% or more for at least 4 hours after administration of AG14361 (Fig. 3). The acutely toxic effects, found with other PARP-1 inhibitors, were not observed in AG14361-treated mice. AG14361 at well-tolerated doses increased the antitumor activity of temozolomide threefold or more in LoVo xenograft tumors, and the combination resulted in complete remission of SW620 xenograft tumors. The addition of AG14361 increased the antitumor activity of both irinotecan and fractionated x-irradiation approximately twofold in both LoVo and SW620 xenografts (Fig. 5). Alternative strategies to increase the antitumor activity of temozolomide by inhibiting the DNA repair protein O^6-alkylguanine DNA alkyltransferase (ATase) have been reported *(43)*. Unlike ATase inhibitors, which can only sensitize cells proficient in mismatch repair *(44)*, AG14361 increased the activity of temozolomide in mismatch repair-deficient LoVo cells *in vitro* and *in vivo*. Because AG14361 doubled the radiation-induced tumor-growth delay, PARP-1 inhibition may be an effective alternative to other radiosensitization approaches, such as the use of bioreductively activated drugs *(45,46)* or the inactivation or inhibition of epidermal growth factor receptor tyrosine kinase *(47,48)*. Moreover, at radiosensitizing doses, AG14361 was nontoxic alone or in combination with radiation therapy.

AG14361 did not increase the antiproliferative effect of temozolomide in SW620 cells *in vitro* (Fig. 4, A), but the combination of AG14361 and temozolomide resulted in the complete regression of SW620 xenografts (Fig. 5, B). SW620 cells are hypersensitive to temozolomide by virtue of low ATase levels and mismatch repair proficiency *(49,50)*, because resistance to DNA alkylating agents is associated with both high ATase and loss of mismatch repair [for respective reviews, *see (51)* and *(52)*]. Similar studies have shown that, whereas 3-aminobenzamide and another base excision repair inhibitor (methoxyamine) can sensitize mismatch repair-deficient cells to temozolomide *(53,54)*, 3-aminobenzamide is ineffective in cells that are hypersensitive to temozolomide because of low ATase activity and mismatch repair proficiency *(53,55)*. The marked increase in the antitumor activity of temozolomide against SW620 xenografts by coadministration of AG14361 may arise from an effect of AG14361 on the tumor microenvironment. AG14361 increased transient perfusion (Fig. 6), potentially altering the microdistribution and delivery of chemotherapeutic agents *(56)*. PARP-1 inhibitors may therefore have greater chemosensitizing potential *in vivo* than indicated by the *in vitro* data. Nicotinamide (a weak PARP-1 inhibitor) similarly inhibits contraction of vascular smooth muscle in tumors by a mechanism that does not involve nitric oxide release or Ca^{2+} signaling *(57,58);* nicotinamide is in advanced clinical trials to evaluate its ability to increase sensitivity to radiation therapy *(59)*.

In conclusion, AG14361 is, to our knowledge, the first PARP-1 inhibitor with the pharmacologic properties of high potency, specificity, stability, and *in vivo* activity that are necessary for its use in anticancer chemotherapy and radiation therapy in humans. We describe an improved therapeutic index with AG14361 in combination with temozolomide, irinotecan, and radiation in a human colon tumor xenograft model. Measurement of PARP-1 activity in cells and tissue homogenates provides a reliable and quantitative biomarker to support the performance and evaluation of clinical trials with PARP-1 inhibitors. Such trials should allow a mechanism-based evaluation of PARP-1 inhibition as a therapeutic treatment for cancer and could be a major step forward in the development of chemotherapy directed at the DNA-damage response of cancer cells.

REFERENCES

(1) Smith S. The world according to PARP. Trends Biochem Sci 2001;26:174–9.

(2) de Murcia G, Menissier de Murcia J. Poly(ADP-ribose) polymerase: a molecular nick-sensor [published erratum appears in Trends Biochem Sci 1994;19:250]. Trends Biochem Sci 1994;19:172–6.

(3) Dantzer F, de La Rubia G, Menissier-De Murcia J, Hostomsky Z, de Murcia G, Schreiber V. Base excision repair is impaired in mammalian cells lacking Poly(ADP-ribose) polymerase-1. Biochemistry 2000;39:7559–69.

(4) Tentori L, Portarena I, Graziani G. Potential clinical applications of poly(ADP-ribose) polymerase (PARP) inhibitors. Pharmacol Res 2002;45:73–85.

(5) Griffin RJ, Curtin NJ, Newell DR, Golding BT, Durkacz BW, Calvert AH. The role of inhibitors of poly(ADP-ribose) polymerase as resistance-modifying agents in cancer therapy. Biochimie 1995;77:408–22.

(6) Barret JM, Hill BT. DNA repair mechanisms associated with cellular resistance to antitumor drugs: potential novel targets. Anticancer Drugs 1998;9:105–23.

(7) Satoh MS, Lindahl T. Role of poly(ADP-ribose) formation in DNA repair. Nature 1992;356:356–8.

(8) Curtin NJ, Golding BT, Griffin RJ, Newell DR, Roberts MJ, Srinivasan S, et al. New PARP inhibitors for chemo- and radio-therapy of cancer. In: deMurcia G, Shall S, editors. From DNA damage and stress signalling to cell death: poly ADP-ribosylation reactions. Oxford (U.K.): Oxford University Press; 2000. p. 177–206.

(9) Molinete M, Vermeulen W, Burkle A, Menissier-de Murcia J, Kupper JH, Hoeijmakers JH, et al. Overproduction of the poly(ADP-ribose) polymerase DNA-binding domain blocks alkylation-induced DNA repair synthesis in mammalian cells. EMBO J 1993;12:2109–17.

(10) Ding R, Smulson M. Depletion of nuclear poly(ADP-ribose) polymerase by antisense RNA expression: influences on genomic stability, chromatin organization, and carcinogen cytotoxicity. Cancer Res 1994;54:4627–34.

(11) de Murcia JM, Niedergang C, Trucco C, Ricoul M, Dutrillaux B, Mark M, et al. Requirement of poly(ADP-ribose) polymerase in recovery from DNA damage in mice and in cells. Proc Natl Acad Sci U S A 1997;94:7303–7.

(12) Purnell MR, Whish WJ. Novel inhibitors of poly(ADP-ribose) synthetase. Biochem J 1980;185:775–7.

(13) Suto MJ, Turner WR, Arundel-Suto CM, Werbel LM, Sebolt-Leopold JS. Dihydroisoquinolinones: the design and synthesis of a new series of potent inhibitors of poly(ADP-ribose) polymerase. Anticancer Drug Des 1991;6:107–17.

(14) Banasik M, Komura H, Shimoyama M, Ueda K. Specific inhibitors of poly(ADP-ribose) synthetase and mono(ADP-ribosyl)transferase. J Biol Chem 1992;267:1569–75.

(15) Bowman KJ, White A, Golding BT, Griffin RJ, Curtin NJ. Potentiation of anti-cancer agent cytotoxicity by the potent poly(ADP-ribose) polymerase inhibitors NU1025 and NU1064. Br J Cancer 1998;78:1269–77.

(16) Bowman KJ, Newell DR, Calvert AH, Curtin NJ. Differential effects of the poly (ADP-ribose) polymerase (PARP) inhibitor NU1025 on topoisomerase I and II inhibitor cytotoxicity in L1210 cells in vitro. Br J Cancer 2001;84:106–12.
(17) Delaney CA, Wang LZ, Kyle S, White AW, Calvert AH, Curtin NJ, et al. Potentiation of temozolomide and topotecan growth inhibition and cytotoxicity by novel poly(adenosine diphosphoribose) polymerase inhibitors in a panel of human tumor cell lines. Clin Cancer Res 2000;6: 2860–7.
(18) Tentori L, Leonetti C, Scarsella M, d'Amati G, Portarena I, Zupi G, et al. Combined treatment with temozolomide and poly(ADP-ribose) polymerase inhibitor enhances survival of mice bearing hematologic malignancy at the central nervous system site. Blood 2002;99:2241–4.
(19) Canan Koch SS, Thoresen LH, Tikhe JG, Maegley KA, Almassy RJ, Li J, et al. Novel tricyclic poly(ADP-ribose) polymerase-1 inhibitors with potent anticancer chemopotentiating activity: design, synthesis, and X-ray cocrystal structure. J Med Chem 2002;45:4961–74.
(20) Skalitzky DJ, Marakovits JT, Maegley KA, Ekker A, Yu XH, Hostomsky Z, et al. Tricyclic benzimidazoles as potent poly(ADP-ribose) polymerase-1 inhibitors. J Med Chem 2003;46:210–3.
(21) Robertson EJ. Embryo-derived stem cell lines. In: Robertson EJ, editor. Teratocarcinomas and embryonic stem cells: a practical approach. Oxford (U.K.): IRL Press, Ltd.; 1987. p. 71–112.
(22) Chen TR. In situ detection of mycoplasma contamination in cell cultures by fluorescent Hoechst 33258 stain. Exp Cell Res 1977;104:255–62.
(23) Jung S, Miranda EA, de Murcia JM, Niedergang C, Delarue M, Schulz GE, et al. Crystallization and X-ray crystallographic analysis of recombinant chicken poly(ADP-ribose) polymerase catalytic domain produced in Sf9 insect cells. J Mol Biol 1994;244:114–6.
(24) Brunger AT, Adams PD, Clore GM, DeLano WL, Gros P, Grosse-Kunstleve RW, et al. Crystallography & NMR system: a new software suite for macromolecular structure determination. Acta Crystallogr D Biol Crystallogr 1998;54(Pt 5):905–21.
(25) Mohamadi F, Richards NG, Guida WC, Liskamp R, Lipton M, Caufield C, et al. Macromodel-an integrated software system for modeling organic and bioorganic molecules using molecular mechanics. J Comp Chem 1990;11: 440–67.
(26) Marsischky GT, Wilson BA, Collier RJ. Role of glutamic acid 988 of human poly-ADP-ribose polymerase in polymer formation. Evidence for active site similarities to the ADP-ribosylating toxins. J Biol Chem 1995; 270:3247–54.
(27) Grube K, Küpper JH, Bürkle A. Direct stimulation of poly(ADP-ribose) polymerase in permeabilised cells by double-stranded DNA oligomers [published erratum appears in Anal Biochem 1991;195:378]. Anal Biochem 1991;193:236–9.
(28) Skehan P, Storeng R, Scudiero D, Monks A, McMahon J, Vistica D, et al. New colorimetric cytotoxicity assay for anticancer-drug screening. J Natl Cancer Inst 1990;82:1107–12.
(29) Wodicka L, Dong H, Mittmann M, Ho MH, Lockhart DJ. Genome-wide expression monitoring in Saccharomyces cerevisiae. Nat Biotechnol 1997; 15:1359–67.
(30) Sandberg R, Yasuda R, Pankratz DG, Carter TA, Del Rio JA, Wodicka L, et al. Regional and strain-specific gene expression mapping in the adult mouse brain. Proc Natl Acad Sci U S A 2000;97:11038–43.
(31) Lockhart DJ, Dong H, Byrne MC, Follettie MT, Gallo MV, Chee MS, et al. Expression monitoring by hybridization to high-density oligonucleotide arrays. Nat Biotechnol 1996;14:1675–80.
(32) Potter GW. Analysis of biological molecules: an introduction to principles, instrumentation and techniques. 1st ed. London (U.K.): Chapman and Hall; 1995. p. 202.
(33) Thomas CD, Stern S, Chaplin DJ, Guichard M. Transient perfusion and radiosensitizing effect after nicotinamide, carbogen, and perflubron emulsion administration. Radiother Oncol 1996;39:235–41.
(34) Mendoza-Alvarez H, Alvarez-Gonzalez R. Poly(ADP-ribose) polymerase is a catalytic dimer and the automodification reaction is intermolecular. J Biol Chem 1993;268:22575–80.
(35) Leopold W, Sebolt-Leopold JS. Chemical approaches to improve radiotherapy. In: Valeriote FA, Corbett TH, Baker LH, editors. Cytotoxic anticancer drugs: models and concepts for drug discovery and development. Boston (MA): Kluwer Academic Publishers; 1992. p. 179–96.
(36) Weichselbaum RR, Little JB. The differential response of human tumours to fractionated radiation may be due to a post-irradiation repair process. Br J Cancer 1982;46:532–7.
(37) Newlands ES, Stevens MF, Wedge SR, Wheelhouse RT, Brock C. Temozolomide: a review of its discovery, chemical properties, pre-clinical development and clinical trials. Cancer Treat Rev 1997;23:35–61.
(38) Horsman MR. Nicotinamide and other benzamide analogs as agents for overcoming hypoxic cell radiation resistance in tumours. A review. Acta Oncol 1995;34:571–87.
(39) Berthet N, Boturyn D, Constant JF. DNA repair inhibitors. Expert opinion on therapeutic patents. 1999;9:401–15.
(40) Martin DS, Stolfi RL, Nord LD, Colofiore JR. Enhancement of chemotherapeutically-induced apoptosis in vivo by biochemical modulation of poly(ADP-ribose) polymerase. Oncol Rep 1996;3:317–22.
(41) Virag L, Szabo C. The therapeutic potential of poly(ADP-ribose) polymerase inhibitors. Pharmacol Rev 2002;54:375–429.
(42) Barendsen GW, Van Bree C, Franken NA. Importance of cell proliferative state and potentially lethal damage repair on radiation effectiveness: implications for combined tumor treatments (review). Int J Oncol 2001;19: 247–56.
(43) Middleton MR, Thatcher N, McMurry TB, McElhinney RS, Donnelly DJ, Margison GP. Effect of O6-(4-bromothenyl)guanine on different temozolomide schedules in a human melanoma xenograft model. Int J Cancer 2002;100:615–7.
(44) Gerson SL. Clinical relevance of MGMT in the treatment of cancer. J Clin Oncol 2002;20:2388–99.
(45) Patterson LH, McKeown SR, Ruparelia K, Double JA, Bibby MS, Cole S, et al. Enhancement of chemotherapy and radiotherapy of murine tumours by AQ4N, a bioreductively activated anti-tumour agent. Br J Cancer 2000;82:1984–90.
(46) el-Said A, Menke D, Dorie MJ, Brown JM. Comparison of the effectiveness of tirapazamine and carbogen with nicotinamide in enhancing the response of a human tumor xenograft to fractionated irradiation. Radiat Oncol Investig 1999;7:163–9.
(47) Lammering G, Hewit TH, Hawkins WT, Contessa JN, Reardon DB, Lin PS, et al. Epidermal growth factor receptor as a genetic therapy target for carcinoma cell radiosensitization. J Natl Cancer Inst 2001;93:921–9.
(48) Williams KJ, Telfer BA, Stratford IJ, Wedge SR. ZD1839 ('Iressa'), a specific oral epidermal growth factor receptor-tyrosine kinase inhibitor, potentiates radiotherapy in a human colorectal cancer xenograft model. Br J Cancer 2002;86:1157–61.
(49) Arris CE. The evaluation of novel inactivators of O6-methyl-guanine-DNA methyltransferase. [PhD thesis]. Newcastle upon Tyne (U.K.): Univ. of Newcastle upon Tyne; 1998.
(50) Aquilina G, Ceccotti S, Martinelli S, Hampson R, Bignami M. N-(2-chloroethyl)-N′-cyclohexyl-N-nitrosourea sensitivity in mismatch repair-defective human cells. Cancer Res 1998;58:135–41.
(51) Kaina B, Christmann M. DNA repair in resistance to alkylating anticancer drugs. Int J Clin Pharmacol Ther 2002;40:354–67.
(52) Margison GP, Santibanez Koref MF, Povey AC. Mechanisms of carcinogenicity/chemotherapy by O6-methylguanine. Mutagenesis 2002;17: 483–7.
(53) Wedge SR, Porteous JK, Newlands ES. 3-aminobenzamide and/or O6-benzylguanine evaluated as an adjuvant to temozolomide or BCNU treatment in cell lines of variable mismatch repair status and O6-alkylguanine-DNA alkyltransferase activity. Br J Cancer 1996;74:1030–6.
(54) Taverna P, Liu L, Hwang HS, Hanson AJ, Kinsella TJ, Gerson SL. Methoxyamine potentiates DNA single strand breaks and double strand breaks induced by temozolomide in colon cancer cells. Mutat Res 2001; 485:269–81.
(55) Lunn JM, Harris AL. Cytotoxicity of 5-(3-methyl-1-triazino)imidazole-4-carboxamide (MTIC) on Mer+, Mer+Rem- and Mer- cell lines: differential potentiation by 3-acetamidobenzamide. Br J Cancer 1988;57:54–8.
(56) Kamm YJ, Heerschap A, Wagener DJ. Effect of carbogen breathing on the pharmacodynamics of 5-fluorouracil in a murine colon carcinoma. Eur J Cancer 2000;36:1180–6.
(57) Hirst DG, Kennovin GD, Flitney FW. The radiosensitizer nicotinamide inhibits arterial vasoconstriction. Br J Radiol 1994;67:795–9.

(58) Burns DM, Ruddock MW, Walker MD, Allen JM, Kennovin GD, Hirst DG. Nicotinamide-induced vasoconstriction: lack of dependence on agonist signalling pathways. Eur J Pharmacol 1999;374:213–20.
(59) Kaanders JH, Bussink J, van der Kogel AJ. ARCON: a novel biology-based approach in radiotherapy. Lancet Oncol 2002;3:728–37.

NOTES

Editor's note: Agouron Pfizer approved this manuscript. R. Almassy, Z. Hostomsky, J. Li, K. Maegley, and D. Skalitsky hold stock in Pfizer, owner of AG14361. A. H. Calvert, N. J. Curtin, and D. R. Newell are eligible for an employee reimbursement of a fraction of any royalty paid to the University of Newcastle upon Tyne should a PARP inhibitor from this program generate such royalty. I. J. Stratford and K. J. Williams are conducting research sponsored by Agouron Pfizer.

Supported by Cancer Research UK (formerly Cancer Research Campaign).

We are grateful to M. North (Pfizer) for the gene array analysis data, to Brian Telfer (Manchester) for excellent technical assistance, and to Josiane Menissier-de Murcia and Gilbert de Murcia for supplying PARP-$1^{-/-}$ and PARP-$1^{+/+}$ mice.

Manuscript received April 9, 2003; revised October 22, 2003; accepted November 10, 2003.